

Tip-over Stability Control for a Holonomic Omnidirectional Mobile Robot with Active Dual-wheel Caster Assemblies using SGCMG

M. Juhairi Aziz Safar^{1,2}, Keigo Watanabe¹, Shoichi Maeyama¹ and Isaku Nagai¹

Abstract—In this paper, we present the tip-over prevention technique using a control moment gyro for a holonomic omnidirectional mobile robot with active dual wheel caster assemblies. With concern to the sudden dynamic changes during maneuver, the dynamical model is derived and used together with the force-angle stability measure (FASM) to estimate the tip-over incident and the tipping direction. A single gimbal control moment gyro (SGCMG) is proposed to counter the instability by producing a precession torque in the opposite direction of the estimated tip-over direction. Simulation results are given to demonstrate the performance of this approach.

I. INTRODUCTION

Nowadays, the service robots play a big role in human environments to serve the humans and assist them in their daily life. Most of these robots are involved directly with the human whether as a mobile transporter or an assistant robot. There are two major concerns to be realized by the service robots for a better adaptation in human environment which are: (1) the capability to maneuver with high mobility even in crowd and narrow spaces, and (2) to provide a stable maneuver even in the existing of dynamical effects such as instant braking or acceleration. The simplest way to obtain the required mobility is by providing a holonomic omnidirectional locomotion system. Numbers of design have been introduced such as universal or Mecanum wheels [1], orthogonal wheels [2], chains of spherical or cylindrical wheels [3] and ball wheels [4]. Most of these wheels acquire a special design which leads to a complicated structure, discontinuous ground contact and lack of traction power. Therefore, the implementation of standard tires into a holonomic omnidirectional mechanism [5], [6] is more desirable to solve the issues.

The second concern can be realized by enhancing the stability using special mechanisms, controlling systems or just by adding the width and casters. However, extra casters or passive wheels are not the main solution because the dynamical effects still exist. There are several existing methods to measure and evaluate the stability such as static stability margin (SSM) [7], static stability factor (SSF) [8], energy stability margin (ESM) [9], force-angle stability measure (FASM) [10] and a few more variances of these metrics [11], [12]. The SSM and SSF only consider the statically stability aspect. The SSM is widely used in the multi-legged

mobile robots with slow motion assumption, while the SSF is used in the conventional car-like vehicle which is restricted to a quadrilateral shaped support polygon. The FASM has advantages over other dynamical stability measures due to a simple calculation and a top-heavy sensitive measure. These metrics incorporate with control system to provide the tip-over prevention such mentioned in [13]. A control moment gyro (CMG) is a torque generator for attitude control of an artificial satellite in space [14] and in naval vessel [15]. In both cases, the CMG is use as an actuator to produce instantaneous torque to control the attitude or prevent the instability. In ground vehicle applications, the CMG usually is paired with the dynamics model or inverted pendulum model especially in two-wheeled vehicle to provide the balancing [16]. Currently, there is no example of application for more complicated footprint.

In this paper, we present a tip-over prevention system for a holonomic omnidirectional mobile robot with active dual-wheel caster assemblies. The dynamical model is derived to find the relationship of the wheels reaction forces in the existence of the dynamical effects. With the combination of FASM, the tip-over stability is measured and the tip-over axis is predicted. The CMG is used to overcome the instability by providing the gyroscopic torque in the opposite direction of the estimated tip-over direction. Some simulations were conducted to verify the effectiveness of this system.

II. OMNIDIRECTIONAL MOBILE ROBOT

A. Kinematical Model

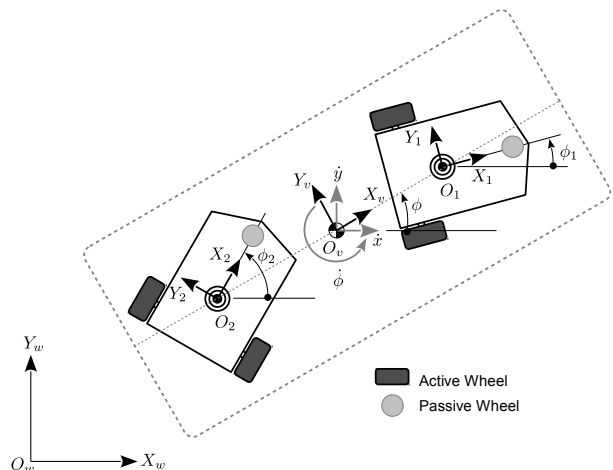


Fig. 1. Omnidirectional mobile robot with ADWC assemblies

¹Department of Intelligent Mechanical Systems, Division of Industrial Innovation Sciences, Graduate School of Natural Science and Technology, Okayama University, 3-1-1 Tsushima-naka, Kita-ku, Okayama 700-8530, Japan. juhairi@usmm.sys.okayama-u.ac.jp

² School of Mechatronic Engineering, Universiti Malaysia Perlis, Pauh Putra Campus, 02600 Arau, Perlis, Malaysia

The proposed omnidirectional transport mobile robot in our study is shown in Fig. 1. This mobile robot is capable to produce a holonomic motion of three degrees of freedom at the center of the mobile robot, O_v . The holonomic motion is produced by the two units of active dual-wheel caster assemblies (ADWCs) which are arranged in the longitudinal direction of the mobile robots' body. Each unit of the ADWC is capable to drive a two degrees of freedom (2-DOF) motion at the steering axle in the forward direction (X_i -axis) and sideway direction (Y_i -axis). The details of the kinematics equation has been presented in [6].

B. Dynamic Support Polygon

Unlike a specialized wheel omnidirectional mobile robot and a car-like vehicle, this mobile robot possess a dynamic footprint or support polygon. Due to the rapid changes in the ADWCs orientation, the support polygon in a same robot orientation has unlimited possible shapes which vary from four to six edges polygon. However, with the assumption of a uniform trajectory plane, the number of contact points were maintained as long as in a stable state. The examples of the support polygon according to a given trajectory and motion is shown in Fig. 2.

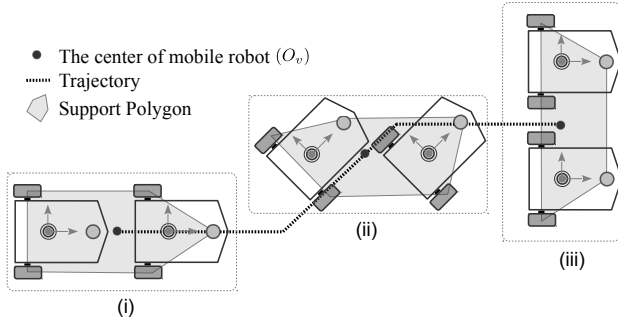


Fig. 2. Support polygon

This dynamic support polygon can be described at any instant by the convex hull solution of set $S \in \mathbb{R}^2$ which contain N points (p_1, p_2, \dots, p_N) , where the convex hull P_{ch} is given by

$$P_{ch} \triangleq \left\{ \sum_{j=1}^N \lambda_j p_j : \lambda_j \geq 0 \text{ for all } j \text{ and } \sum_{j=1}^N \lambda_j = 1 \right\}.$$

Each point p_j in set S is assigned a coefficients so that the coefficients are all positive and sum to one. These coefficients are used to compute an average weight of the points. The convex hull is formed when all the intersection of all convex set for the coefficients is solved.

C. Tip-over axis and tip-over angle

The tip-over axis on which the tip-over incident takes place can be on any edge of the support polygon. However, the candidate for the tip-over axis can sometimes exist on more than one axis. For example, if the mobile robot move in a straight trajectory with the pose (i) as shown in Fig. 2, the

candidate of the tip-over axis may exist on two edges of the support polygon; the right and the left of the mobile robot. However, at any tip-over incident, only one edge is involved, e.g. when unexpected disturbances or braking exist. The tip-over direction can be obtained by finding the perpendicular line from the center of mass to the estimated tip-over axis. Meanwhile, the tip-over angle is defined as the angle between the tip-over direction and the X_v -axis. More details about the tip-over axis and the tip-over angle are provided in section IV.

III. DYNAMICAL MODEL

The dynamical model of our omnidirectional transport mobile robot is shown in Fig. 3 and Fig. 4. The loads can be exist as a human driver, container or any weight. In term of simplicity, the load is defined as a cuboid shape. Assume the center of mass (CoM) for the SGCMG and the mobile platform are the same. With the assumption that the total of mass for the mobile platform including the SGCMG as M_p and the loads as M_l , the total mass for the upper part of the mobile robot can be summed up as $M_a = M_p + M_l$.

Defining the mobile robot pose in the Σ_w system as $\mathbf{x} = [x \ y \ \phi]^T$, the supporting forces for each ADWC as $\mathbf{f}_{iz} = [f_{zri} \ f_{zli} \ f_{zfi}]^T$ and the overall supporting forces as $\mathbf{f}_z = [f_{1z} \ f_{2z}]^T$, the equations of the dynamical model can be derived by

$$\mathbf{f}_z = \mathbf{Q}\dot{\mathbf{x}} + \mathbf{R}\ddot{\mathbf{x}} + \mathbf{D} \quad (1)$$

where,

$$\mathbf{Q} = \mathbf{B}(\dot{\mathbf{F}}\mathbf{G}^* + \mathbf{F}\mathbf{G}^*), \mathbf{R} = (\mathbf{A}\mathbf{E}^* \mathbf{M} + \mathbf{B}\mathbf{F}\mathbf{G}^* + \mathbf{K}).$$

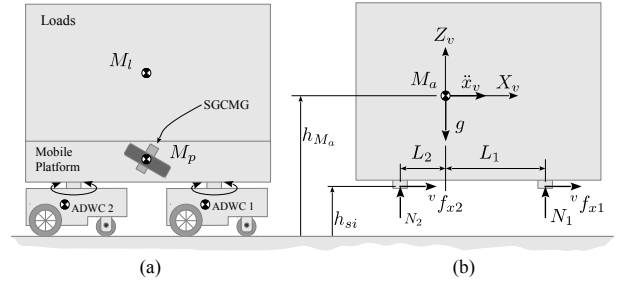


Fig. 3. (a) Overview of the omnidirectional mobile robot with loads, (b) Dynamical model of upper part of the mobile robot

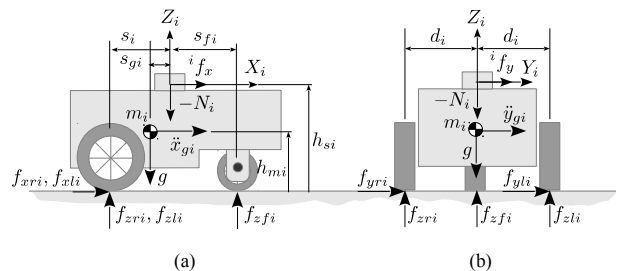


Fig. 4. Dynamical model of lower part of the mobile robot

$$\begin{aligned}
\mathbf{B} &= \begin{bmatrix} \mathbf{B}_1 & \mathbf{0}_{3 \times 2} \\ \mathbf{0}_{3 \times 2} & \mathbf{B}_2 \end{bmatrix}, \mathbf{B}_i = \begin{bmatrix} \frac{m_i h_{mi}}{2s_{ci}} & \frac{m_i h_{mi} s_{ai}}{2d_i} \\ \frac{m_i h_{mi}}{2s_{ci}} & -\frac{m_i h_{mi} s_{ai}}{2d_i} \\ -\frac{m_i h_{mi}}{s_{ci}} & 0 \end{bmatrix} \\
\mathbf{F} &= \begin{bmatrix} \mathbf{F}_1 & \mathbf{0}_{2 \times 2} \\ \mathbf{0}_{2 \times 2} & \mathbf{F}_2 \end{bmatrix}, \mathbf{F}_i = \begin{bmatrix} C_i & S_i \\ -\frac{1}{s_i} S_i & \frac{1}{s_i} C_i \end{bmatrix} \\
\mathbf{G}^* &= \begin{bmatrix} 1 & 0 & -L_1 \sin \phi \\ 0 & 1 & L_1 \cos \phi \\ 1 & 0 & L_2 \sin \phi \\ 0 & 1 & -L_2 \cos \phi \end{bmatrix}, \mathbf{A} = \begin{bmatrix} \mathbf{A}_1 & \mathbf{0}_{3 \times 2} \\ \mathbf{0}_{3 \times 2} & \mathbf{A}_2 \end{bmatrix} \\
\mathbf{A}_i &= \begin{bmatrix} \frac{h_{ci}}{2s_{ci}} C_i + \frac{h_{ci}}{2d_i} S_i & -\frac{h_{ci}}{2s_{ci}} S_i + \frac{h_{ci}}{2d_i} C_i \\ \frac{h_{ci}}{2s_{ci}} C_i - \frac{h_{ci}}{2d_i} S_i & -\frac{h_{ci}}{2s_{ci}} S_i - \frac{h_{ci}}{2d_i} C_i \\ -\frac{1}{s_{ci}} C_i & \frac{1}{s_{ci}} S_i \end{bmatrix} \\
\mathbf{K} &= \frac{M_a h_a}{L} \begin{bmatrix} \frac{s_{f1}}{2s_{c1}} C_1 & -\frac{s_{f1}}{2s_{c1}} S_1 & 0 \\ \frac{s_{f1}}{2s_{c1}} C_1 & -\frac{s_{f1}}{2s_{c1}} S_1 & 0 \\ \frac{s_1}{s_{c1}} C_1 & -\frac{s_1}{s_{c1}} S_1 & 0 \\ -\frac{s_{f2}}{2s_{c2}} C_2 & \frac{s_{f2}}{2s_{c2}} S_2 & 0 \\ -\frac{s_{f2}}{2s_{c2}} C_2 & \frac{s_{f2}}{2s_{c2}} S_2 & 0 \\ -\frac{s_2}{s_{c2}} C_2 & \frac{s_2}{s_{c2}} S_2 & 0 \end{bmatrix} \\
\mathbf{E}^* &= \frac{1}{L} \begin{bmatrix} L_2 + \alpha_{cc}(\phi) & \alpha_{sc}(\phi) & -\sin \phi \\ \alpha_{sc}(\phi) & L_2 + \alpha_{ss}(\phi) & \cos \phi \\ L_1 - \alpha_{cc}(\phi) & -\alpha_{sc}(\phi) & \sin \phi \\ -\alpha_{sc}(\phi) & L_1 - \alpha_{ss}(\phi) & -\cos \phi \end{bmatrix} \\
&\alpha_{ss}(\phi) = \frac{1}{2}(L_1 - L_2) \sin^2 \phi \\
&\alpha_{sc}(\phi) = \frac{1}{2}(L_1 - L_2) \sin \phi \cos \phi \\
&\alpha_{cc}(\phi) = \frac{1}{2}(L_1 - L_2) \cos^2 \phi \\
\mathbf{D} &= g \begin{bmatrix} \frac{m_1 s_{b1}}{2s_{c1}} - \frac{s_{f1} M_a L_2}{2s_{c1} L} \\ \frac{m_1 s_{b1}}{2s_{c1}} - \frac{s_{f1} M_a L_2}{2s_{c1} L} \\ \frac{m_1 s_{a1}}{s_{c1}} - \frac{s_1 M_a L_2}{s_{c1} L} \\ \frac{m_2 s_{b2}}{2s_{c2}} - \frac{s_{f2} M_a L_1}{2s_{c2} L} \\ \frac{m_2 s_{b2}}{2s_{c2}} - \frac{s_{f2} M_a L_1}{2s_{c2} L} \\ \frac{m_2 s_{a2}}{s_{c2}} - \frac{s_2 M_a L_1}{s_{c2} L} \end{bmatrix} \\
\mathbf{M} &= \text{diag}(M_a, M_a, I_z), L = L_1 + L_2 \\
s_{ai} &= s_i - s_{gi}, s_{bi} = s_{fi} + s_{gi}, s_{ci} = s_i + s_{fi}, \\
h_{ci} &= 2h_{mi} - h_{si}, C_i = \cos \phi_i, S_i = \sin \phi_i
\end{aligned}$$

The details of the derivation can be referred in our previous work in [17].

IV. TIP-OVER PREDICTION

The tip-over prediction can be described by the illustration shown in Fig. 5. The dynamic equilibrium of forces at the CoM can be obtained using the Newtonian principles by

$$\begin{aligned}
\mathbf{f}_r &= \Sigma \mathbf{f}_g + \Sigma \mathbf{f}_d - \Sigma \mathbf{f}_{in} \\
&= -\Sigma \mathbf{f}_s
\end{aligned} \quad (2)$$

where subscripts r, g, d, in and s denote the net force, gravitational, external disturbances, inertial and support forces, respectively. Thus, the net force, \mathbf{f}_r , can easily be obtained if all

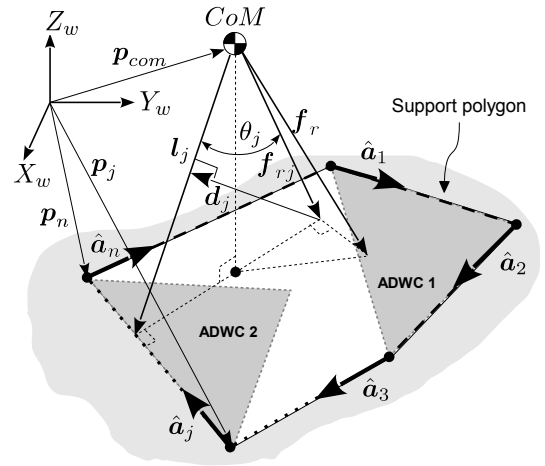


Fig. 5. Tip-over stability measurement by FASM

support forces are known. In the case of stationary condition, the value of \mathbf{f}_s is equal to the ground reaction forces which caused by the gravitational force only. In our approach, the net force can be estimated from the z -axis value of the \mathbf{f}_s which obtained using the above mentioned dynamical model. The tip-over incident is predicted based on the minimum value of the FASM stability metric for each edge of the support polygon. Defining the component of the net force perpendicular to the j -th edge of the support polygon as \mathbf{f}_{rj} , the angle between the \mathbf{f}_{rj} and the line from CoM to the tip-over axis as θ_j , and the distance d_j , the FASM stability metric for tip-over incident can be measured by

$$\beta = \min_j (\theta_j \cdot \| \mathbf{d}_j \| \cdot \| \mathbf{f}_{rj} \|) \quad j = (1, \dots, n). \quad (3)$$

Here, the positive magnitude of β indicates the tip-over stability margin of a stable system. The stability of the mobile robot reached at the critical condition when one of the component becoming zero, where the tip-over stability margin $\beta = 0$.

The estimated tip-over direction is described by the tip-over angle, α as shown in Fig. 6. The positive and negative sign of α indicate the direction of the estimated tip-over axis. The $+\alpha$ shows the estimated tip-over axis exists on the left side of the omnidirectional mobile robot. On the

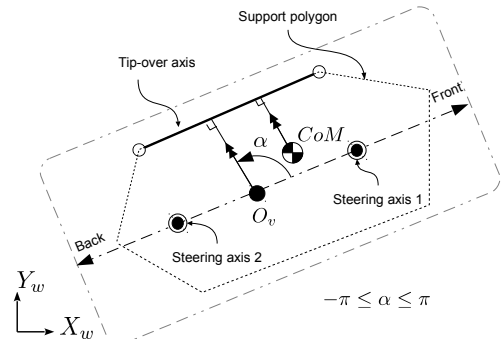


Fig. 6. Estimation of tip-over direction

other hand, the $-\alpha$ shows the right side direction. With the current setting, the mobile robot is estimated to tip-over more on the left or right side of the mobile robot compared with other edges based on the result presented in [17] using the FASM technique. While, the estimated tip-over angle by SSM, α_{SSM} , by simulation is $80.84 \text{ deg} \leq \alpha_{SSM} \leq 99.16 \text{ deg}$ or $-99.16 \text{ deg} \leq \alpha_{SSM} \leq -80.84 \text{ deg}$. The range of the tip-over angle is very small in reference to the Y_v -axis. Therefore it is sufficient to provide a tip-over preventing mechanism that focused on the side tip-over only.

V. SINGLE GIMBAL CONTROL MOMENT GYRO

A control moment gyro (CMG) normally is used as a torque generator for an attitude control of an artificial satellite or for a roll-over control in a ship vessel. The CMG can be classified into two basic types: single gimbal CMG (SGCMG) and double gimbal CMG (DGCMG). The single gimbal system offers mechanical simplicity but enable higher output torque production than the double gimbal system. In comparison to the reaction wheel, the CMG system can produce greater instantaneous torque due to the continuous high speed flywheel which stores high momentum. Due to these advantages, the SGCMG is proposed as the tip-over preventing mechanism for our omnidirectional mobile robot.

A simple SGCMG system consists of a flywheel rotating at a constant speed and one gimbal motor as shown in Fig. 7. The spinning flywheel produces an angular momentum, \mathbf{H}_f , in the z -axis direction. If a rotational precession rate of ω_p is applied to the spinning flywheel about the gimbal axis, a precession output torque, τ_p , which is perpendicular to the direction of vector ω_f and ω_p will be generated.

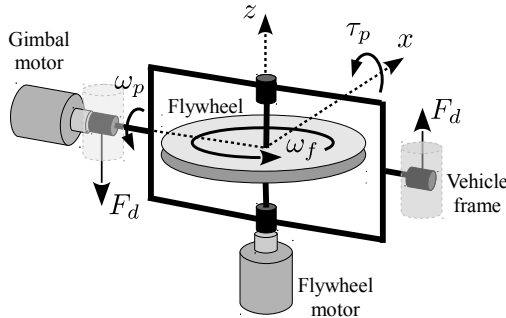


Fig. 7. Single gimbal control moment gyro (SGCMG)

Defining the angular velocity of the spinning flywheel as ω_f and the moment of inertia of the flywheel as I_f , the angular momentum produced by the spinning flywheel in the z -axis is

$$\mathbf{H}_f = I_f \omega_f \quad (4)$$

Thus, the gyroscopic torque produced by the existing rotational precession rate of ω_p is

$$\tau_p = \mathbf{H}_f \omega_p = I_f \omega_f \omega_p \quad (5)$$

The production of this gyroscopic torque induced a force to the center of mass on the y -axis direction which later use to provide a counter force to the predicted tip-over direction.

VI. SIMULATION

The simulations were conducted to demonstrate and verify the effectiveness of the tip-over preventing model as well as the tipping stability prediction method. These simulations were conducted under the resolved velocity control [18]. The simulation time is 10 s and the sampling period is 20 ms. The task of the mobile robot is to transport a load in two simple motions of holonomic omnidirectional mobile robot: (1) translational motion in sideways direction (Y_v -axis), (2) simultaneous translational and rotational motion. Each transport is simulated to start from a stationary position and obtain the maximum velocity of 0.6 m/s after 1 s. In the last second, the mobile robot decelerates to a final stationary stop. The dimension of the load is set to $1.0 \text{ m} \times 0.5 \text{ m} \times 0.8 \text{ m}$ with the weight of 80 kg. Assume that the dimension of the mobile platform is $1.0 \text{ m} \times 0.5 \text{ m} \times 0.1 \text{ m}$. As for the SGCMG unit, the flywheel disc is set as a 2 kg metal disc with a radius of 0.15 m. Other physical parameters of the omnidirectional mobile robot are listed in Table I. Fig. 8 shows the references and responses for the velocity and acceleration.

TABLE I
PHYSICAL PARAMETERS

Parameters	Value	Unit
M_l	80.0	[kg]
M_p	7.0	[kg]
m_1, m_2	6.5	[kg]
L_1	0.30	[m]
L_2	0.35	[m]
h_{s1}, h_{s2}	0.15	[m]
h_{m1}, h_{m2}	0.08	[m]
d_1, d_2	0.13	[m]
r_1, r_2	0.05	[m]
s_1, s_2	0.075	[m]
s_{g1}, s_{g2}	0.0155	[m]
s_{f1}, s_{f2}	0.08	[m]

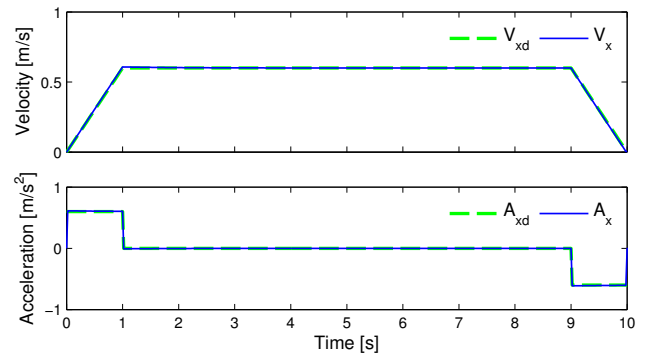


Fig. 8. References and responses of velocity and acceleration

The setting of the driving mode for this simulation are as below:

- 1) Translational motion in sideways direction (Y_v -axis) – the omnidirectional mobile robot is set to move to its sideways direction from an initial pose of $\mathbf{x} =$

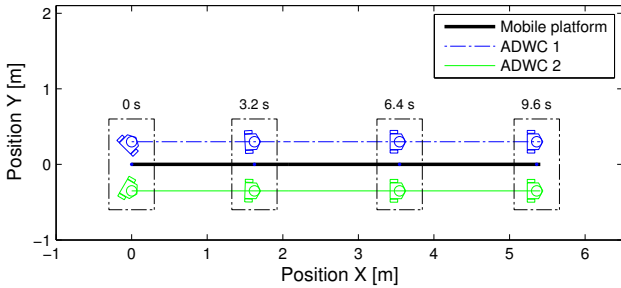
$[0 \ 0 \ \pi/2]^T$, the initial orientation of ADWC1 is set to $\pi/4$ rad and ADWC2 is set to $-\pi/6$ rad.

- 2) Simultaneous translational and rotational motion – the omnidirectional mobile robot is set to move to its longitudinal direction while performing rotation. The initial pose of the omnidirectional mobile robot was set to $\mathbf{x} = [0 \ 0 \ 0]^T$ and the initial orientation of ADWC1 is set to $\pi/2$ rad and ADWC2 is set to $\pi/4$ rad. The additional angular velocity was set to $\pi/20$ rad/s.

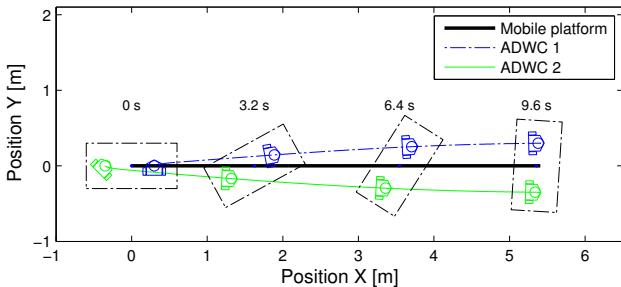
For the sake of similar trajectory responses in the conducted simulation for each situation (subsection A and B), the results for both driving modes are shown only once as illustrated in Fig. 9.

A. CMG control with threshold setting mode

In this simulation, the flywheel disc is set to rotate at a constant velocity of 223.53 rad/s, while the gimbal rotating rate is set to 5 rad/s. The trajectory for both driving mode is stable during the first 9 s but instable in the last second during deceleration as shown by the FASM value in Fig. 10. Both instability occurred in the same direction which the tip-over angle, α , is equal to $\pi/2$ rad. We noticed that the estimated direction is parallel with the minus direction of Y_v -axis or perpendicular to the right side of the vehicle body. In order to increase the power efficiency, the tip-over preventing mechanism only works during the critical instability. During the stable condition the gimbal is set to 0 rad/s. The threshold for the tip-over prevention is set to the lower FASM value to focus on the critical instability only. In this simulation the FASM threshold is set to FASM value below 4. The counter torque from the CMG works in the direction against the tip-over direction and improve the

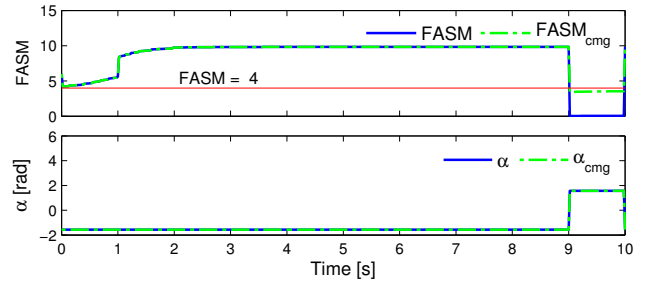


(a) Mode 1: Sideway translational

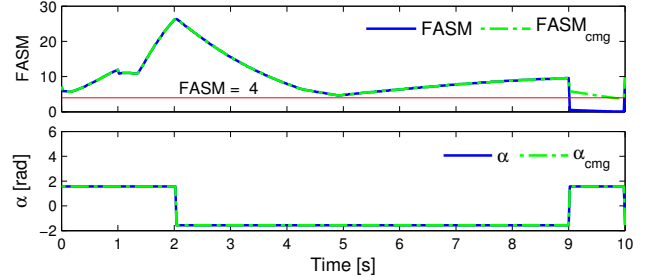


(b) Mode 2: Translational and rotational motion

Fig. 9. Response of the trajectory for both driving mode



(a) Driving mode 1



(b) Driving mode 2

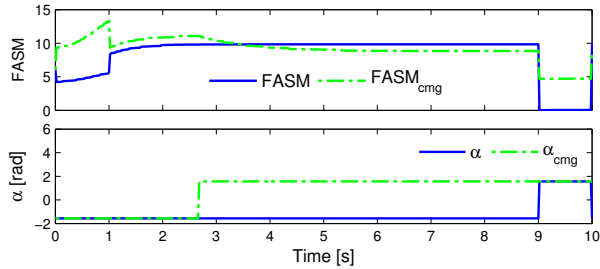
Fig. 10. CMG activation with threshold set to FASM = 4

stability of the mobile robot. The result can be seen from the improved FASM value shown in both driving mode during the final deceleration. The estimated tip-over angle for the improved FASM is maintained.

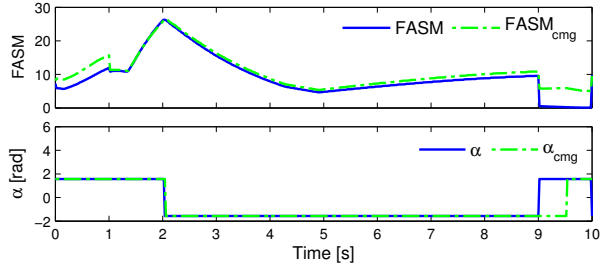
B. Self generated counter CMG mode

In order to generalize and simplify the CMG control, the production of the precession torque is set to a self generation system. The counter torque is produce automatically by the CMG to balance the component of the net-force that is working perpendicular to the predicted tip-over axis. The condition set for this simulation is similar to the previous subsection. As shown in Fig. 11, the FASM value when the CMG is activated, $FASM_{cmg}$, is better compared to the normal FASM value. The stability during the lowest FASM value is improved, thus the possibility of the tip-over incident has decreased. In comparison with the previous result, the CMG also moderate the FASM value in other stable conditions due to the continuous torque production. This changes does not influence the stability of the mobile robot itself, but may lead to the high energy consumption.

The production of the precession torque by the CMG unit can be controlled by choosing the right angular rate for the flywheel disc and the gimbal. As the relation of these angular rates are straight forward, we can produce the same precession torque with several choices of the angular rates. As an example in driving mode 1, by setting the angular rate of the gimbal, ω_p , equal to 5 rad/s, the angular rate for the flywheel disc should be provided as shown in the above chart in Fig. 12(a). On the other hand, the same precession torque can be obtained by setting the ω_f as 200 rad/s and control the ω_p alone as shown in the below chart of Fig. 12(a). Controlling the ω_f is not a good option because to



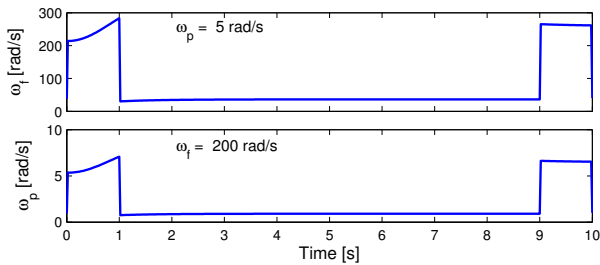
(a) Driving mode 1



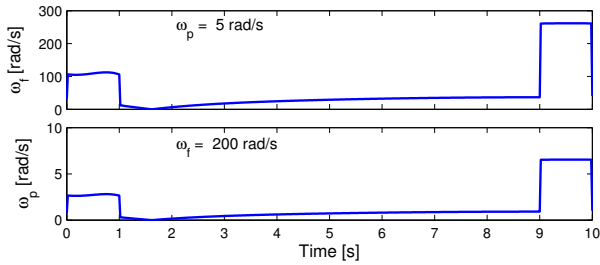
(b) Driving mode 2

Fig. 11. Self generated CMG

increase or decrease a high volume velocity in instant is almost impossible. Therefore, controlling the ω_p instead of ω_f or both of them is more desirable to obtain the highest efficiency and simplicity. The same conclusion can be made from the example of driving mode 2 which is given in Fig. 12(b).



(a) Driving mode 1



(b) Driving mode 2

Fig. 12. Required angular rate for flywheel and gimbal

VII. CONCLUSION

In this paper, we have successfully simulated the omnidirectional transport mobile robot with active dual-wheel caster assemblies. The combination of derived dynamical model and the FASM was used to predict the tip-over occurrence. The effectiveness of the tip-over prevention method was verified through some simulations as presented.

REFERENCES

- [1] B. E. Ilon, "Wheels for a course stable self propelling vehicle movable in any desired direction on the ground or some other base," US Patent 3876255, Apr. 8, 1975.
- [2] F. G. Pin and S. M. Killough, "A new family of omnidirectional and holonomic wheeled platforms for mobile robots," *IEEE Trans. on Robot. and Autom.*, vol. 10, pp. 480–489, 1994.
- [3] R. Damoto, W. Cheng, and S. Hirose, "Holonomic omnidirectional vehicle with new omni-wheel mechanism," *Proc. IEEE Int. Conf. on Robot. and Autom.*, 2001, pp. 773–778.
- [4] K. Tadakuma, R. Tadakuma and J. Berengeres, "Development of holonomic omnidirectional vehicle with "omni-ball": spherical wheels," *Proc. IEEE Int. Conf. on Intell. Robots and Systems*, Oct./Nov. 2007, pp. 33–39.
- [5] M. J. A. Safar, K. Watanabe, S. Maeyama and I. Nagai, "A study of tipping stability for omnidirectional mobile robot with active dual-wheel caster assemblies," *J. Artificial Life and Robotics*, vol. 17, no. 1, pp. 145–151, Oct 2012.
- [6] T. Yamada, K. Watanabe, K. Kiguchi and K. Izumi, "Dynamic model and control for a holonomic omnidirectional mobile robot," *J. Autonomous Robots*, vol. 11, pp. 73–189, 2001.
- [7] R. McGhee and G. Iswandhi, "Adaptive locomotion for a multilegged robot over rough terrain," *IEEE Trans. Systems, Man, and Cybernetics* vol. 9, no. 4, pp. 176–182, 1979.
- [8] U. S. Government, *Trends in static stability factor of passengers cars, light trucks and vans*, 2005.
- [9] D. A. Messuri, C. A. Klein, "Automatic body regulation for maintaining stability of a legged vehicle during rough-terrain locomotion," *IEEE J. Robotics and Autom.*, vol. 1, no. 3, pp. 132–141, Sep. 1985.
- [10] E. G. Papadopoulos, D. A. Rey, "The force-angle measure of tipover stability margin for mobile manipulators," *J. Vehicle System Dynamics* vol. 33, pp. 29–48, 2000.
- [11] Q. Huang, S. Sugano and I. Kato, "Stability control for a mobile manipulator using a potential method," *Proc. IEEE Int. Conf. Intell. Robots and Systems*, Sep. 1994, pp. 839–846.
- [12] S. Hirose, H. Tsukagoshi and K. Yoneda, "Normalized energy stability margin and its contour of walking vehicles on rough terrain," *Proc. IEEE Int. Conf. Robotics and Autom.*, May 2001, vol. 1, pp. 181–186.
- [13] S. H. Ken, N. Moshchuk, F. Nardi and J. Ryu, "Vehicle rollover avoidance," *IEEE Control System Magazine*, pp. 70–85, 2010.
- [14] H. Kurokawa, "A geometric study of single gimbal control moment gyros - singularity problems and steering law," *Technical Report, Mechanical Engineering Laboratory, Japan*, no. 175, Jan. 1998.
- [15] N. C. Townsend, A. J. Murphy, R. A. Sheno, "A new active gyro-stabiliser system for ride control of marine vehicles," *Ocean Engineering*, vol. 34, no. 11/12, pp. 1607–1617, 2007.
- [16] A. V. Beznos, A. M. Formal'sky, E. V. Gurfinkel et al., "Control of autonomous motion of two-wheel bicycle with gyroscopic stabilisation," *Proc. IEEE Int. Conf. on Robotics and Autom.*, May 1998, vol. 3, pp. 2670–2675.
- [17] M. J. A. Safar, K. Watanabe, S. Maeyama, I. Nagai, "Tip-over prediction for omnidirectional mobile robot," *Procedia Engineering* vol. 41, pp. 1085–1094, 2012.
- [18] F. Han, T. Yamada, K. Watanabe, K. Kiguchi and K. Izumi, "Construction of an omnidirectional mobile robot platform based on active dual-wheel caster mechanisms and development of a control simulator," *J. Intell. and Robotic Systems*, vol. 29, pp. 257–275, 2000.